LBL-13302
Preprint

Lawrence Berkeley Laboratory

UNIVERSITY OF CALIFORNIA

Physics, Computer Science & Mathematics Division

RECEIVED
LAWRENCE
BERKELEY LABORATORY

OCT 26 1981

LIBRARY AND
DOCUMENTS SECTION

To be submitted for publication

A FRONT TRACKING METHOD APPLIED TO BURGERS' EQUATION AND TWO-PHASE POROUS FLOW

Per Lötstedt

October 1981

TWO-WEEK LOAN COPY

This is a Library Circulating Copy which may be borrowed for two weeks. For a personal retention copy, call Tech. Info. Division, Ext. 6782

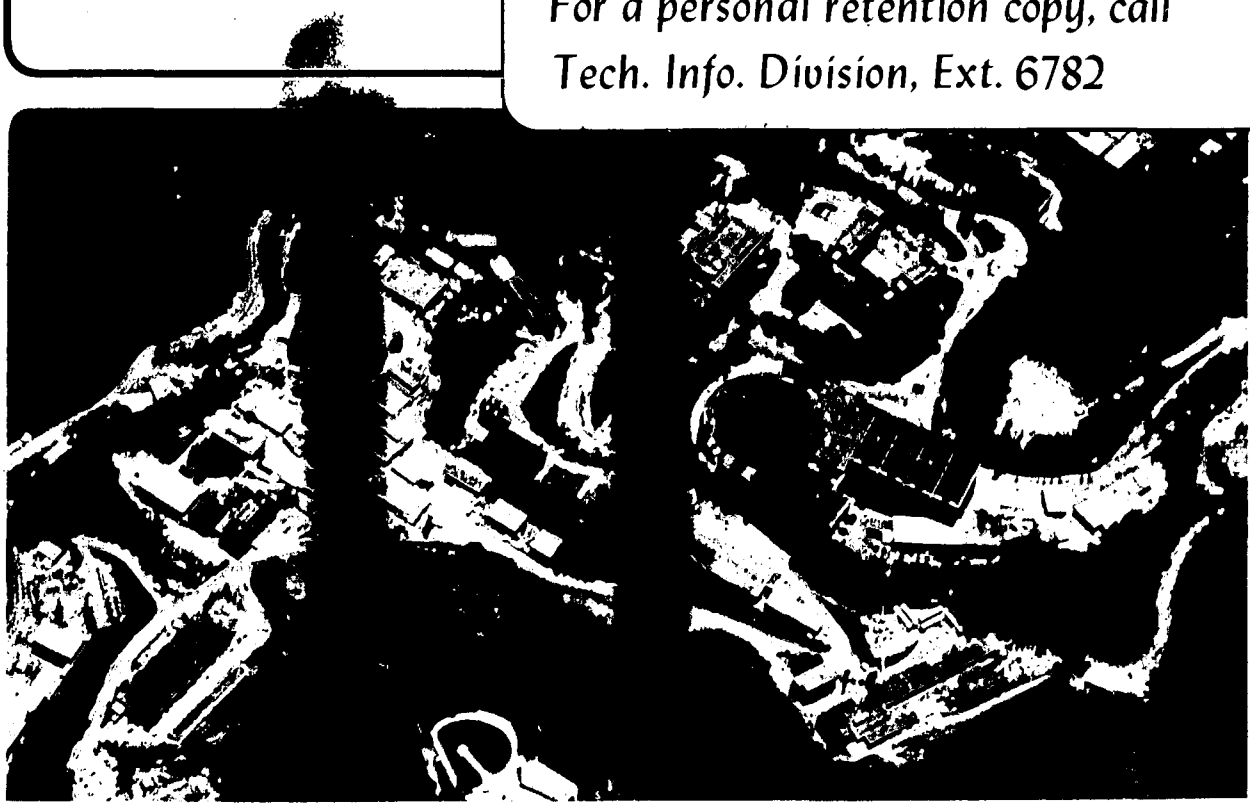

LBL-13302 c.2

Prepared for the U.S. Department of Energy under Contract W-7405-ENG-48

DISCLAIMER

This document was prepared as an account of work sponsored by the United States Government. While this document is believed to contain correct information, neither the United States Government nor any agency thereof, nor the Regents of the University of California, nor any of their employees, makes any warranty, express or implied, or assumes any legal responsibility for the accuracy, completeness, or usefulness of any information, apparatus, product, or process disclosed, or represents that its use would not infringe privately owned rights. Reference herein to any specific commercial product, process, or service by its trade name, trademark, manufacturer, or otherwise, does not necessarily constitute or imply its endorsement, recommendation, or favoring by the United States Government or any agency thereof, or the Regents of the University of California. The views and opinions of authors expressed herein do not necessarily state or reflect those of the United States Government or any agency thereof or the Regents of the University of California.

LBL-13302

A FRONT TRACKING METHOD APPLIED TO BURGERS' EQUATION AND TWO-PHASE POROUS FLOW

Per Lötstedt

Lawrence Berkeley Laboratory
University of California
Berkeley, California 94720

AMS (MOS) Subject Classification (1980): 65M99, 76S05, 76T05

This work was supported in part by the Director,
Office of Energy Research, Office of Basic Energy Sciences,
Engineering, Mathematical, and Geosciences Division
of the U. S. Department of Energy under Contract No. W-7405-ENG-48

A FRONT TRACKING METHOD APPLIED TO BURGERS' EQUATION AND TWO-PHASE POROUS FLOW

Per Lötstedt

Lawrence Berkeley Laboratory
University of California
Berkeley, California 94720

Abstract

A method is presented that is capable of following discontinuities in the solution of hyperbolic partial differential equations. At every time-step for each cell in the neighborhood of the discontinuity the fraction of the cell lying behind the discontinuity curve is updated. From this data the front is reconstructed. The method is applied to three differential equations: inviscid Burgers' equation, the Buckley-Leverett equation for immiscible porous flow and the equation for two-phase miscible flow in a porous medium.

1. Introduction

Discontinuities in the solution of hyperbolic partial differential equations appear in many physical applications, e.g., gas dynamics, flame propagation and petroleum reservoir simulation. Methods to follow these time-dependent fronts in two space dimensions have been described by Richtmyer and Morton [17] and more recently by Noh and Woodward [15], Chorin [3], Glimm, Isaacson, Marchesin and McBryan [11] and Hirt and Nichols [14]. The last reference contains a review of several front tracking techniques. In Refs. [17] and [11] the discontinuity curve is approximated by a number of points. The front is advanced in time by moving the points with the front speed, either in the direction normal to the front [17] or along the characteristics [11]. Another way of representing the front is suggested in Refs. [15], [14] and [3]. For each mesh cell covering the domain of the solution the fraction F of the cell that lies behind the front is stored. F satisfies $0 \leq F \leq 1$ and consequently, $1 - F$ is the fraction of the cell that lies ahead of the front. Using this information an approximate line of discontinuity can be constructed. The fractions are transported by a velocity field $v = (v_x, v_y)$ determined by the position of the front and the particular hyperbolic equation to be solved. The fractions are moved in two steps: one in the x-direction using v_x and one in the y-direction using v_y. At each step the part of the volume behind the front in every cell that flows over a grid line to an adjacent cell is determined. Then the fractional values are updated. The approach taken here is a development of these latter ideas presented in Ref. [15] and [3].

The front tracking method is applied here to the numerical solution of three examples of scalar hyperbolic partial differential equations (PDEs),

$$u_t + \nabla\cdot(qf(u)) = 0 \quad , \tag{1.1}$$

with discontinuous initial data on the domain $(x,y) \in \Omega = [0,1] \times [0,1]$. The front speed is given by the Rankine-Hugoniot condition and the velocity field $q = (q_x, q_y)$. The three hyperbolic PDEs are inviscid Burgers' equation, the Buckley-Leverett equation and the equation for porous, two-phase, miscible flow:

1. Inviscid Burgers' Equation

$$\begin{aligned} &u_t + \nabla\cdot(1/2\, qu^2) = 0 \quad , \\ &q(x,y) = (1,1) \quad . \end{aligned} \tag{1.2}$$

2. The Buckley-Leverett Equation

$$\begin{aligned} &u_t + \nabla\cdot(qf(u)) = 0 \quad , \\ &\partial u/\partial n = 0 \quad \text{on } \partial\Omega, \text{ the boundary of } \Omega,\ u(t,0,0) = 1, \end{aligned} \tag{1.3a}$$

$$q = -\lambda(u)\,\nabla p \quad ,$$

(1.3b)

$$\nabla\cdot(\lambda(u)\,\nabla p) = g \quad , \quad \partial p/\partial n = 0 \quad \text{on } \partial\Omega.$$

The fractional flow function f(u) and the total mobility $\lambda(u)$ are taken to be

$$f(u) = u^2/(u^2 + \alpha(1-u)^2) \quad , \quad \alpha \in (0,1] \quad ,$$

(1.3c)

$$\lambda(u) = u^2 + \alpha(1-u)^2 \quad .$$

3. The equation for porous two-phase miscible flow,

$$u_t + \nabla\cdot(qu) = 0 \quad ,$$

(1.4a)

$$\partial u/\partial n = 0 \quad \text{on} \quad \partial\Omega, u(t,0,0) = 1 \quad .$$

The value of q satisfies Eq. (1.3b) and $\lambda(u)$ has the definition

(1.4b) $$\lambda(u) = (u + \beta(1-u))^4 \quad , \quad \beta > 0 \quad .$$

The initial data for Burgers' equation is such that the solution contains both shocks and rarefaction waves. The saturation u for the flow of two immiscible, incompressible fluids through a homogeneous porous medium satisfies the Buckley-Leverett equation if the effects of

gravity and capillary pressure are negligible. The quantity p is the pressure and α is the viscosity ratio between the two phases. There holds $g(x,y) = 0$ except for a source at (0,0) and a sink at (1,1), both of unit strength. Equations (1.3) and (1.4) are of importance in the simulation of petroleum reservoirs, see Peaceman [16].

The hyperbolic equations (1.2), (1.3a) and (1.4a) are solved by operator splitting. Glimm's method or the upstream difference method combined with Godunov's method is used for the integration of the continuous parts of the solution. The solution to the elliptic equation (1.3b) for the porous flow examples is obtained at each time-step by a finite difference approximation.

2. The Front Tracking Method

Place a uniform square grid of mesh spacing h in the x- and y-direction over the domain Ω of interest. Suppose that a value of v is available everywhere in Ω. For each mesh cell (i,j) define the value F_{ij} to be the fraction of the cell that is behind the front. The discussion is simplified if the region behind the front henceforth is identified as the "black fluid" and the region ahead of the front is identified as the "white fluid."

At each time-step the fractions in the mesh cells are moved using v in two one-dimensional steps, first in the x-direction and then in the y-direction. A local approximation of the interface between black and white fluid is performed in each cell (i,j) for which $0 < F_{ij} < 1$ before the fluid in the cell is moved in a coordinate direction. This approximation is based on F in the neighboring cells and is not necessary for the majority of the cells for which $F_{ij} = 0$ or $F_{ij} = 1$. The interpretation of the front in the x-direction may be different from that in the y-direction.

In order to construct a local front in a cell (i,j) for a step in the horizontal direction it is sufficient to consider the three cases in Fig. 1. The conditions on F in the neighboring cells in each case are:

Case 1 (Fig. 1.1): $F_4 \neq 0$ and $F_5 = 0$

and

$((F_2 \neq 0 \text{ or } F_3 \neq 0) \text{ or } (F_7 \neq 0 \text{ or } F_8 \neq 0))$,

Case 2 (Fig. 1.2): $((F_4 \neq 0 \text{ and } F_5 \neq 0) \text{ or } F_4 = F_5 = 0)$

and

$F_7 > F_2$,

Case 3 (Fig. 1.3): $F_4 \neq 0$

and

$F_7 \neq 0$

and

$F_2 = F_3 = F_5 = 0$.

The other nine possible configurations satisfy conditions that are easily derived by moving the triangle in Case 3 to the other three corners and by interchanging the role of black and white. If none of the cases above applies then Case 1 is chosen if $F_4 \geq F_5$, and if $F_5 > F_4$ the opposite case is chosen.

The slope of the interface is determined as follows:

Case 1: The upper and lower edge, x_u and x_d, of the trapezoid are proportional to F_2 and F_7,

$$\frac{x_u}{x_d} = \left(\frac{F_2}{F_7}\right)^z \quad , \quad z \in [0,1] \quad , \tag{2.1}$$

and satisfy the area condition

$$0.5h(x_u + x_d) = h^2 F_{ij} \quad . \tag{2.2}$$

If Eqs. (2.1) and (2.2) imply that $x_u > h$ ($x_d > h$) then solve Eq. (2.2) for x_d (x_u) with $x_u = h$ ($x_d = h$).

Case 2: This case is equivalent to Case 1 with F_2 and F_7 in Eq. (2.1) replaced by F_4 and F_5.

Case 3: Let a right triangle T have its two perpendicular sides on the grid lines and the right angle at the lower left corner of the cell (i,j). Let x_T and y_T be the lengths of the sides in the x- and y-direction, respectively. Compute x_T and y_T such that

$$\frac{x_T}{y_T} = \left(\frac{F_7}{F_4}\right)^z \quad , \tag{2.3}$$

$$0.5\ x_T y_T = h^2 F_{ij} \quad . \tag{2.4}$$

If $x_T \leq h$ and $y_T \leq h$ then take x_d and y_ℓ, the left edge of the triangle in Fig. 1.3, to be x_T and y_T. Otherwise, determine T such that Eq. (2.3) is satisfied and the area of T inside the cell is $h^2 F_{ij}$. This polygonal area contains the black fluid.

The value of z in Eqs. (2.1) and (2.3) is 0,0.5 or 1.0 in the numerical examples. Noh and Woodward [15] allow only interfaces parallel to the grid. Chorin [3] introduces black and white rectangles inside the mesh cells to increase the accuracy. With z = 0 the local front line in Cases 1 and 2 is parallel to the mesh.

When the interface between the black and white fluid has been established, the fluids in a cell are advected with the velocity $v_x(x,y)$. The timestep taken at time t_n to advance the front is k.

Case 1: Let v_u and v_d be the values of v_x at t_n along the upper and lower mesh line, respectively. Then

$$x_u(t_n + k) = x_u(t_n) + v_u k \quad ,$$

$$x_d(t_n + k) = x_d(t_n) + v_d k \quad .$$

If $x_u(t_n + k) > h$ or $x_d(t_n + k) > h$ then determine the volume of black fluid ΔF_{ij} that has entered the right cell and update F_{ij} and $F_{i,j+1}$,

$$F_{ij}(t_n + k) = F_{ij}(t_n) - \Delta F_{ij} \quad ,$$

$$F_{i,j+1}(t_n + k) = F_{i,j+1}(t_n) + \Delta F_{ij} \quad .$$

Proceed in a similar manner if $x_u(t_n + k) < 0$ or $x_d(t_n + k) < 0$. If $v_\ell = 0.5(v_u + v_d) < 0$ then the contribution to the left cell is $-v_\ell k$. If $F_{i,j-1} = 1$ and $v_\ell > 0$ then the cell (i,j) receives $\Delta F_{ij} = v_\ell k$ from its left neighbor.

Case 2: Let v_ℓ and v_r be the values of v_x at the left and right boundaries of the cell. Depending on the signs of v_ℓ and v_r the original trapezoid is stretched or contracted and advected. The parallel edges remain constant. Then the possible contributions to the cells (i,j-1) and (i,j+1) are computed.

Case 3: Stretch or contract the triangle with v_u at the left edge and v_d at the lower right corner. Then decide if any black fluid has moved into the left or right cell.

For each cell F_{ij} must fulfill $0 \leq F_{ij} \leq 1$. Hence, if $F_{ij}(t_n + k) > 1$ then $F_{ij}(t_n + k) = 1$ and if $F_{ij}(t_n + k) < 0$ then $F_{ij}(t_n + k) = 0$. To prevent the black fluid in a cell from flowing in one direction into more than one neighboring cell, k must satisfy the restriction

$$k \leq h/|v| \quad . \tag{2.5}$$

The domain Ω of the solution in the numerical experiments is $[0,1] \times [0,1]$ with Neumann boundary conditions or with the directional derivative $\partial u/\partial s = 0$ on $\partial\Omega$, $s = x - y$. The grid on Ω is augmented by extra rows and columns so that the area $[-h,1+h] \times [-h,1+h]$ is covered. When one sweep in a coordinate direction is completed, the values of F in the extra cells outside of Ω are determined by reflection. Thus, all cells in Ω have a left and right neighbor as required by the algorithm.

In order to compute the solution of the differential equation using the information on the front available from the front tracking method, the position of the discontinuities on the grid lines must be calculated. If the front crosses a horizontal line with black fluid to the left and white fluid to the right, two possibilities are distinguished, see Fig. 2.

Case 1 (Fig. 2.1): $F_3 = F_6 = 0$, $F_k \neq 0$, $k = 1,2,4,5$. The discontinuity point on line j is approximated by

$$x = x_i + 0.5h(F_2 + F_5) \quad . \tag{2.6}$$

Case 2 (Fig. 2.2): $F_3 = 0$, $F_k \neq 0$, $k = 1,2,4,5,6$. The approximation of the discontinuity point on line j is

$$x = x_i + 0.5h(F_2 + F_5 + F_6) \quad . \tag{2.7}$$

By using Eq. (2.7), a mesh point lying behind the front in the coordinate direction will also do that in the other direction. When the order of black and white at the front is reversed the formulas (2.6) and (2.7) are modified correspondingly.

The coordinates of the discontinuities and their character (black-left or black-right) are stored for each line in the horizontal and vertical directions in vectors for later use when the differential equation is solved. The coordinates are connected to form the front curve in the graphical output. Knowledge of the character of a discontinuity on a line simplifies the task of following its path in time.

It is possible that e.g. a previous shock wave is replaced by a rarefaction wave due to a reversal of the flow or, as in two of the examples, that an initial discontinuity develops into a rarefaction wave. Whether such a wave starts in a cell (i,j) or not is determined by the hyperbolic PDE and the normal to the constructed front line. The

contributions to neighboring cells ΔF_{ij} are computed as before but F_{ij} is held constant.

The front tracking method requires extra memory to store the $O(1/h^2)$ components of F_{ij}. Computational experience (cf Fenimore [8]) indicates that the zone of cells at the front for which $0 < F_{ij} < 1$ is seldom more than two cells wide. Thus, the number of front cells for which calculations are necessary at each time-step is $O(1/h)$. Evidently the formulas (2.6) and (2.7) for computing the points of discontinuity on a grid line are at least $O(h)$ accurate for exact values F_{ij}. However, for straight lines the error is sometimes proportional to h. Hence, the accuracy of Eqs. (2.6) and (2.7) is $O(h)$. Fenimore [8] demonstrates that the errors introduced in F_{ij} by Noh and Woodward's method [15] in a special case are of first order.

With a simplified procedure for computing the local interfaces the method can be extended to problems in three spatial dimensions. The discontinuity point on a grid line is then determined by the values of F in the four surrounding rows of grid cubes.

The approximate values of u and q in Eq. (1.1), u^n and q^n, are known at grid points and on grid lines as displayed in Fig. 3. For the equation (1.1) the velocity field v for advection of the front cells is given by q and the Rankine-Hugoniot condition. In each of the three cases in Fig. 1 v_x is computed as follows:

Case 1 (Fig. 1.1): Let u_o and u_1 be the values of u^n surrounding the closest discontinuity on the upper grid line. Furthermore, let q_* be the value of q_x on the upper edge of the cell (i,j). Then

$$v_u = q_*(f(u_1) - f(u_o))/(u_1 - u_o) \quad . \tag{2.8}$$

v_d is determined in a similar way.

Case 2 (Fig. 1.2): Let u_o and u_1 be the values of u^n surrounding the closest discontinuity on the left grid line. Let q_* be the value of q_x on the lower edge of the cell. Then v_ℓ is given by the same expression as v_u in Eq. (2.8). v_r is calculated from u_o and u_1 on the right grid line and q_*.

Case 3 (Fig. 1.3): Case 3 is equivalent to Case 1.

3. Time-Integration of the Differential Equations

The values of p^n, $q^n = (q^n_x, q^n_y)$ and u^n at the points depicted in Fig. 3 are calculated by the following procedures.

p^n in the two-phase flow equations satisfies a finite difference approximation of the elliptic equation (1.3b). The derivative $\partial(\lambda(u)\ \partial p/\partial x)/\partial x$ is replaced by

$$(3.1) \qquad (\lambda_{i+1/2,j}(p_{i+1,j} - p_{ij}) - \lambda_{i-1/2,j}(p_{ij} - p_{i-1,j}))/h^2 \quad ,$$

where $\lambda_{i+1/2,j} = 0.5(\lambda(u^n_{ij}) + \lambda(u^n_{i+1,j}))$ or if u is discontinuous between x_i and x_{i+1} then let $u^n_* = \max(u^n_{ij}, u^n_{i+1,j})$ and $\lambda_{i+1/2,j} = \lambda(u^n_*)$. This choice of u^n_* is particularly suitable here since a thin finger of the least viscous fluid with width less than h containing the point (i,j) will have influence on λ and p. $\lambda_{i-1/2,j}$ is defined in a similar manner and the counterpart of Eq. (3.1) in the y-direction is derived analogously. The resulting system of linear equations is solved by the preconditioned conjugate gradient method, as described in Albright and Concus [1]. The values of q^n_x and q^n_y are approximated by standard difference formulas.

Assume that u^n and q^n are known at t_n. At $t_{n+1} = t_n + k$, u^{n+1} is obtained in two steps by operator splitting, see Richtmyer and Morton [17]. First solve

$$(3.2) \qquad u_t + q_x \frac{\partial}{\partial x}(f(u)) = 0 \quad ,$$

followed by

$$(3.3) \qquad u_t + q_y \frac{\partial}{\partial y} (f(u)) = 0 \quad .$$

The algorithm for computing $u^{n+1/2}$ from Eq. (3.2) in a sweep in the horizontal direction is:

(i) Determine the old points of discontinuity on all the lines in the horizontal direction.

(ii) Transport the black and white fluids using v_x and the method described in the previous section.

(iii) Determine the new points of discontinuity on all the lines in the horizontal direction.

(iv) Compute the continuous parts of $u^{n+1/2}$ on each line by a temporal one-step method, taking both the old and new points of discontinuity into account.

With $u^{n+1/2}$ as input in Eq. (3.3), u^{n+1} is computed in a sweep in the vertical direction. In three space dimensions an additional step in the z-direction is taken.

The last step above requires further comments. The methods chosen in the examples are the upstream difference method combined with Godunov's method, Richtmeyer and Morton [17], Colella [5], and a modified Glimm's method (or piecewise sampling method, random choice method, uniform sampling method) without a staggered grid due to Colella [5]. The random choice method for the solution of the Buckley-Leverett equation (1.3) was first used by Concus and Proskurowski [7]. The upstream difference formula used here for advancing the solution of Eq. (1.1) one time-step in the x-direction is

$$(3.4) \qquad u_{ij}^{n+1/2} = u_{ij}^{n} - \frac{k}{h} q_{i-1/2r,j}^{n}(f(u_{ij}^{n}) - f(u_{i-r,j}^{n})) \quad ,$$

where $r = 1$ ($r=-1$) if $q_{i-1/2,j}^{n}$ and $q_{i+1/2,j}^{n}$ are both positive (negative). If $q_{i-1/2,j}^{n}$ and $q_{i+1/2,j}^{n}$ have different signs then $u_{ij}^{n+1/2}$ is computed with Godunov's method. The upper bound for the stepsize k for stability in Eq. (3.4) and Godunov's method is

$$(3.5) \qquad k \leq h/|qf'(u)| \quad ,$$

and in Glimm's method

$$(3.6) \qquad k \leq 0.5h/|qf'(u)| \quad .$$

Upstream differencing and Godunov's method are first order accurate [17] and the order of Glimm's method approaches first order, Colella [4]. Eqs. (3.2) and (3.3) specify a first order splitting scheme.

Consider a part of a grid line in Fig. 4 with two discontinuities at t_n between which the solution is continuous. A value u^*_5 is extrapolated from u^n_3 and u^n_4,

$$(3.7) \qquad u^*_5 = u^n_4 + (u^n_4 - u^n_3) \quad .$$

The values u^n_i, i=1, ..4, and u^*_5 are then used by one of the above mentioned methods to produce $u_i^{n+1/2}$, i=1, ...5. $u_i^{n+1/2}$, i=6,7... are determined by u^n_i, i=5,6,... . The modified Glimm's method does not

always provide solution values at boundary points or mesh points close to a discontinuity. The missing values are calculated with Eq. (3.4). At a discontinuity point q is assumed to have constant sign so that Eq. (3.4) can be used. For the equation

$$u_t + vu_x = 0 \quad , \quad v=\text{constant} \quad ,$$

computing $u_5^{n+1/2}$ by extrapolation (Eqs. (3.7) and (3.4)) is equivalent to following the characteristics, along which u is constant. If a rarefaction wave starts in a front cell then the point of discontinuity in the cell is ignored. There has been no indication of instability in the front values in the numerical test runs.

Let $\Omega_o(t) \in \Omega$ be the set such that if $(x,y) \in \Omega_o(t)$ then $u(t,x,y) = 0$. Moreover, let $\Omega_1(t)$ be the set $\Omega_1 = \Omega \backslash \Omega_o$. The initial data for Eqs. (1.2), (1.3) and (1.4) is such that $\Omega_o(0) \neq \emptyset$. The hyperbolic PDEs have the following property: if $u_{ij} = 0$ and the point (i,j) is not reached by the front at $t_{n+1/2}$ then $u_{ij}^{n+1/2} = 0$. Hence, no computation is required to update many values of $u_{ij}^{n+1/2}$. $\Omega_1(t)$ grows with the expansion of the shock front. There is no wave interaction between the advancing front and the material ahead of the front.

4. Numerical Results

The numerical solutions to Eqs. (1.2), (1.3) and (1.4) with discontinuous initial data obtained by the method described in the previous two sections are presented and discussed here. All the examples are solved on a square grid with $h = 1/40$ and k fulfills Eq. (2.5) and Eq. (3.5) or (3.6). Glimm's method was used for Eqs. (1.2) and the upstream difference method for Eqs. (1.3) and (1.4). In the figures the development of $\partial\Omega_1^n$, the approximation of the contour of $\Omega_1(t_n)$, is drawn for every example. The initial $\Omega^o{}_1 = \Omega_1(0)$ is in the lower, left corner. Δt is the difference in time between the contours. Only non-zero values of u^n are printed.

The exact solution to Burgers' equation (1.2) is easily derived also in two spatial dimensions. After a simple transformation of the independent variables, Eq. (1.2) becomes a one dimensional problem with known solution. Recently, Eq. (1.2) with discontinuous initial data has been solved numerically by Gropp [12] with a method based on mesh refinement.

The initial data for Eq. (1.2) in the numerical experiments is $u(0,x,y) = 1$, $(x,y) \in \Omega_1(0)$. The boundary conditions are of Neumann type $\partial u/\partial n = 0$ except for Fig. 6 where $\partial u/\partial s = 0$, $s = x - y$. Different random numbers in Glimm's method are used in the two fractional steps Eqs. (3.2) and (3.3). In Figs. 5 and 6 the initial front line retains its shape where the line is straight and the corners are rounded slightly. Part of the rounding effect, at least initially, is caused by the technique for constructing front curves. The error in the speed of

the flat parts is on the level of the round-off errors. The analytical solution satisfies $u(t,x,y) = 1$, $(x,y) \in \Omega_1(t)$, $t \geq 0$, and the computed solution is $u^n = 1$ in Ω^n_1 and $u^n = 0$ in $\Omega^n_o = \Omega \backslash \Omega^n_1$. The solution of the rarefaction wave example in Figs. 7 and 8 on x=y is compared with the analytical solution in Fig. 9. The agreement is very good. Another example with a rarefaction wave is displayed in Figs. 10 and 11. The original method by Noh and Woodward [15] was tested on the initial data of Fig. 5 but was found to be too inaccurate at the corners of the front. In the absence of round-off errors Chorin's method in [3] yields the exact answer for the problem in Fig. 5. The solution to the problem in Fig. 6 obtained with that method had oscillations in the front in the vicinity of the corners.

Numerical solutions to the Buckley-Leverett equation (1.3) in two space dimensions have been obtained by a number of authors [1,2,9-11,18]. They use the same $f(u)$ and $\lambda(u)$ as in Eq. (1.3c) although other choices are possible. In the five-spot oil flow test problem,Collins [6], water is injected into the source at (0,0) and oil is recovered from the sink at (1,1). u is the saturation of water. A shock front where u is discontinuous propagates from (0,0) toward (1,1). For certain values of α in Eq. (1.3c) the front is stable to small perturbations but for other values the front is unstable and "fingering" of the front occurs. Whether the front is stable or not depends on the mobility ratio M [6,13,9,10]. M has the definition

$$(4.1) \qquad M = \lambda(u_b)/\lambda(u_a) \quad ,$$

where u_b is the value of u immediately behind the front and u_a is the value ahead of the front. In the examples $u_a = 0$. The solution of the Riemann problem at the front yields

$$(4.2) \qquad u_b = (\alpha/(1 + \alpha))^{1/2} \quad ,$$

and therefore,

$$(4.3) \qquad M = 2(1 - (\alpha/(1 + \alpha))^{1/2}) \quad .$$

The front is stable if $M < 1$ and unstable if $M > 1$.

The normal component of q at the front q_n is continuous but the tangential component q_t is discontinuous. When the fractions of black fluid at the front are transported in the horizontal direction by v_x only v_n, the component normal to the front, actually moves the front curve. Even if v_t and q_t advect the fractions of black fluid, they have little effect on a moderately curved front and no effect on a straight front line.

In Figs. 12 and 13, Eq. (1.3) is solved with $\lambda(u)$ = constant = 1 for comparison with the exact solution in [2] for $\alpha = 0.5$, $u_b = 0.577$, $M = 0.845$. In this case q is independent of t and is computed only initially. $\Omega_1(0)$ is a quarter of a circle and $u(0,r) = 1 + ar + br^2$, $u(0,r_o) = u_b = 0.577$, where $r = (x^2 + y^2)^{1/2}$. The front is stable for

$\alpha = 0.5$. The initial data for the example in Fig. 14 is computed starting from the same initial data as in Fig. 12. Then a small disturbance is created on the front. The perturbation disappears in accordance with theory. This is in contrast to the results with $\alpha = 0.1$, $u_b = 0.302$, $M = 1.397$. The initial data is prepared as above. A small perturbation develops into a finger in Figs. 15 and 16. The shock profiles are compared in Fig. 15 and 16 for two different values of z in Eqs. (2.1) and (2.3). The most significant difference is the shape of the finger when the front is close to breakthrough at (1,1). Two small perturbations on the front develop into two fingers in Figs. 17 and 18. However, no spontaneous formation of fingers has been observed from an initially smooth front. This is probably due to the fact that M is not sufficiently large and the inaccuracy of the solution to the elliptic equation (1.3b) near the front. Note that M in Eq. (4.3) satisfies $M \in [2 - \sqrt{2}, 2)$. In the last example another model for flow is used allowing a larger M.

The equations of miscible flow (1.4) have been solved in Ref. [11] using a front tracking technique. The initial data here is such that $u(0,x,y) = 1$, $(x,y) \in \Omega_1(0)$. It follows from Eq. (1.4) that $u(t,x,y) = 1$ when $(x,y) \in \Omega_1(t), t \geq 0$. The mobility ratio is $M = 1/\beta^4$. Fig. 19 displays the solution of Eq. (1.4) with $M = 2$. The front is unstable and a "fingering" effect is clearly visible. The computed solution u^n fulfills $u^n = 1$ in Ω^n_1 and $u^n = 0$ in Ω^n_o. The solution of the same problem in Ref. [11] with the front tracking method described there was depicted as having a stable front curve and no fingers.

The typical CPU time required by a VAX-11/780 under VMS to compute the results in Figs. 7, 16 and 19 is presented in Table I.

5. Conclusions

The front tracking method described in Sections 2 and 3 has been tested on three scalar hyperbolic PDEs with discontinuous initial data. The numerical solution of inviscid Burgers' equation agrees very well with the analytical solution for shock waves and rarefaction waves. The same holds true also for the Buckley-Leverett equation with $\alpha = 0.5$ and $\lambda(u) \equiv 1$ in Eq. (1.3b), when compared with the analytically derived solution. When a small perturbation is introduced on the front curve in the general system (Eq. (1.3)) it grows in the unstable case, $\alpha = 0.1$, and disappears in the stable case, $\alpha = 0.5$. Fingers develop spontaneously when the mobility ratio is unfavorable in the two-phase, miscible flow equation. The method is able to resolve and follow unstable irregularities in the interface between shocked and unshocked fluid. The computer time required for the front tracking is comparable to the time used for the solution of the differential equations.

Acknowledgments

The problem was suggested to me by Alexandre J. Chorin and Paul Concus. I have had illuminating discussions with Phillip Colella on the hyperbolic equations and with Paul Concus on the Buckley-Leverett equation.

This work was supported in part by the Director, Office of Energy Research, Office of Basic Energy Sciences, Engineering, Mathematical, and Geosciences Division of the U. S. Department of Energy under Contract No. W-7405-ENG-48.

References

1. N. Albright and P. Concus, "On Calculating Flows with Sharp Fronts in a Porous Medium," Lawrence Berkeley Laboratory report LBL-9286, 1979.

2. N. Albright, P. Concus and W. Proskurowski, "Numerical Solution of the Multidimensional Buckley-Leverett Equation by a Sampling Method," Society of Petroleum Engineers of AIME paper 7681, 1979.

3. A. J. Chorin, J. Comput. Phys. 35 (1980), 1.

4. P. Colella, Ph. D. Thesis, Department of Mathematics, University of California, Berkeley, 1978.

5. P. Colella, SIAM J. Sci. Stat. Comput., to appear.

6. R. E. Collins, "Flow of Fluids Through Porous Materials," Petroleum Publishing Co., Tulsa, 1976.

7. P. Concus and W. Proskurowski, J. Comput. Phys. 30 (1979), 153.

8. C. Fenimore, Ph. D. Thesis, Department of Mathematics, University of California, Berkeley, 1979.

9. J. Glimm, D. Marchesin and O. McBryan, J. Comput. Phys. 39 (1981), 179.

10. J. Glimm, D. Marchesin and O. McBryan, Comm. Pure and Appl. Math. 34 (1981), 53.

11. J. Glimm, E. Isaacson, D. Marchesin and O. McBryan, Adv. Appl. Math. 2 (1981), 91.

12. W. D. Gropp, SIAM J. Sci. Stat. Comput. 1 (1980), 191.

13. B. Habermann, Trans. AIME 219 (1960), 264.

14. C. W. Hirt and B. D. Nichols, J. Comput. Phys. 39 (1981), 201.

15. W. F. Noh and P. Woodward, in "Proceedings, Fifth Intern. Conf. on Numerical Methods in Fluid Dynamics" (A. I. van de Vooren and P. J. Zandbergen, eds.), Springer, New York, 1976.

16. D. W. Peaceman, "Fundamentals of Numerical Reservoir Simulation," Elsevier, New York, 1977.

17. R. D. Richtmyer and K. W. Morton, "Difference Methods for Initial-Value Problems," 2nd ed., Interscience, New York, 1967.

18. A. Spivak, H. S. Price and A. Settari, Soc. Petr. Eng. J. 17 (1977), 27.

Table I.

Example	Total CPU-time	CPU-time per step	Percentage of total CPU-time a)	b)	c)	d)
Fig. 7	191s	1.27s	14.3	58.3	2.5	25.0
Fig. 16	516s	4.13s	3.7	16.7	63.6	16.0
Fig. 19	2153s	4.49s	6.3	14.9	68.7	10.1

a) Computation of points of discontinuity, front curve and rarefaction squares.

b) Computation of F^n_{ij}.

c) Computation of q^n.

d) Computation of u^n.

Figure Captions

Fig. 1. Three different cases in the procedure for transportation of the fractional volumes.

Fig. 2. Two different cases for determination of the point of discontinuity on grid line j.

Fig. 3. The approximate values of u, p and q are computed at mesh points and grid lines.

Fig. 4. A discontinuity moves on a grid line when time increases. A mesh point is marked by a vertical line and a discontinuity by a cross.

Fig. 5. Burgers' equation, $z = 0.0$, $k = 0.01$, $\Delta t = 20\ k$. The spurious wrinkles at some of the corners are partly caused by the routine for constructing the front line. The best approximation in the corners is achieved with $z = 0.0$.

Fig. 6. Burgers' equation, $z = 0.5$, $k = 0.01$, $\Delta t = 20\ k$.

Fig. 7. Burgers' equation, rarefaction wave, $z = 0.5$, $k = 0.01$, $\Delta t = 15\ k$. The initial configuration $\Omega_1(0)$ is the square in the lower left corner.

Fig. 8. $u(1.5,x,y)$ for the problem in Fig. 7.

Fig. 9. The exact solution (marked by ————) on the diagonal $x-y=0$ is compared with the computed values (marked by o) and the computed front (marked by - - -) in Fig. 8.

Fig. 10. Burgers' equation, rarefaction wave, $z = 0.5$, $k = 0.01$, $\Delta t = 20k$. The initial configuration $\Omega_1(0)$ is the square in the lower, left corner.

Fig. 11. u(1.05,x,y) for the problem in Fig. 10. The top of the front curve is rounded and is about 3% slower than the exact solution. The exact u at the top is approximately 0.83.

Fig. 12. The Buckley-Leverett equation (Eqs. (1.3a) and (1.3b)), with $\lambda(u) = 1$ and $\alpha = 0.5$, $z = 0.5$, $k = 0.005$. Between the first 11 lines $\Delta t = 40\ k$ and between the last 3 lines $\Delta t = 10\ k$.

Fig. 13. u(2.125,x,y) for the problem in Fig. 12 immediately before breakthrough. Breakthrough occurs at $t = 2.13$, about 1-2% later than the analytical solution. u is in good agreement with the saturation contours in [2] when the difference in initial conditions has been taken into account.

Fig. 14. The Buckley-Leverett equation as in Eq. (1.3) with $\alpha = 0.5$, $z = 1.0$, $k = 0.005$. $\Delta t = 40\ k$ between the first 6 lines and $\Delta t = 10\ k$ between the last 5 lines. The initial perturbation disappears.

Fig. 15. The Buckley-Leverett equation as in Eq. (1.3) with $\alpha = 0.1$, $z = 0.5$, $k = 0.004$. $\Delta t = 50\ k$ between the first 3 lines and $\Delta t = 32\ k$ between the last 2 lines. The initial perturbation grows.

Fig. 16. For comparison, the problem in Fig. 15 is rerun with $z = 1.0$. The difference between the two solutions is not great considering the unstable nature of the problem.

Fig. 17. The Buckley-Leverett equation as in Eq. (1.3) with $\alpha = 0.1$, $k = 0.004$, $z = 0.5$. $\Delta t = 50\ k$ between the first 3 lines and $\Delta t = 32\ k$ between the last 2 lines. The two initial perturbations grow.

Fig. 18. u (0.528,x,y) is plotted for the last profile in Fig. 17.

Fig. 19. The equations for two-phase, miscible flow, M = 2.0, k = 0.005, z = 1.0. Δt = 40 k except for the last 2 lines where Δt = 20 k.

Fig. 20. q (2.5,x,y) is displayed for the last profile in Fig. 19.

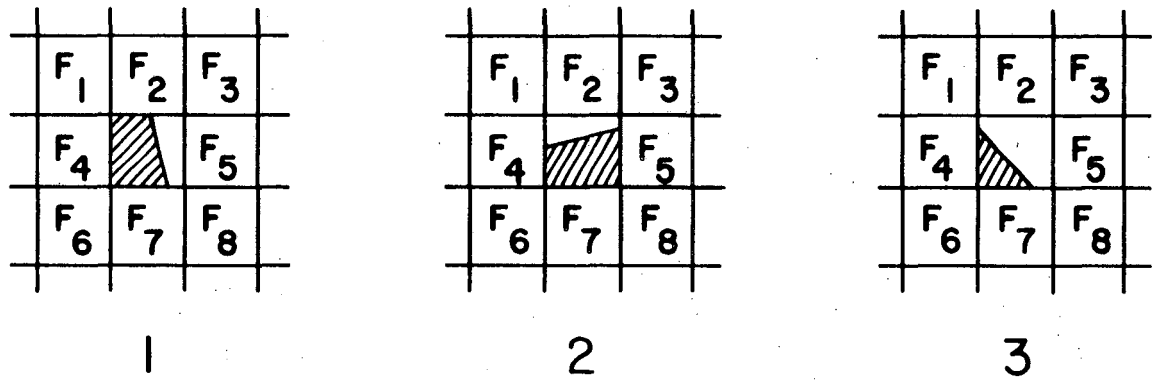

XBL 818-1228

Fig. 1.

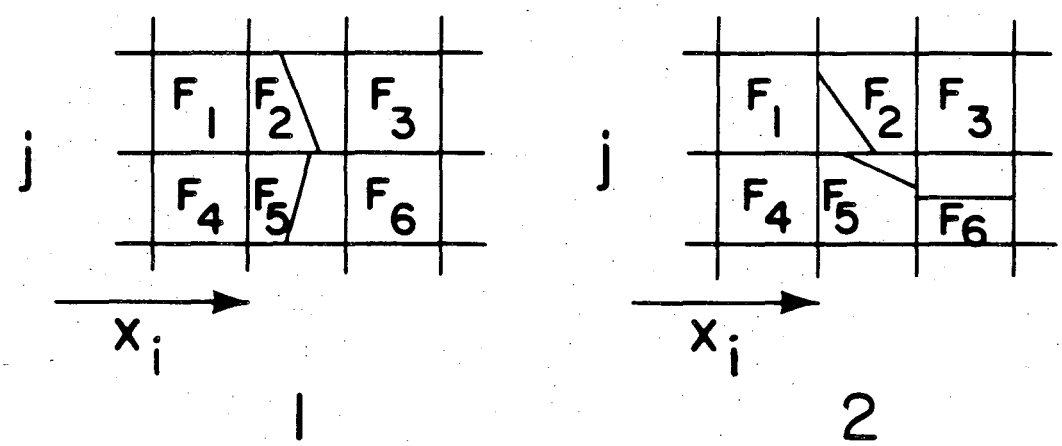

XBL 818-1229

Fig. 2.

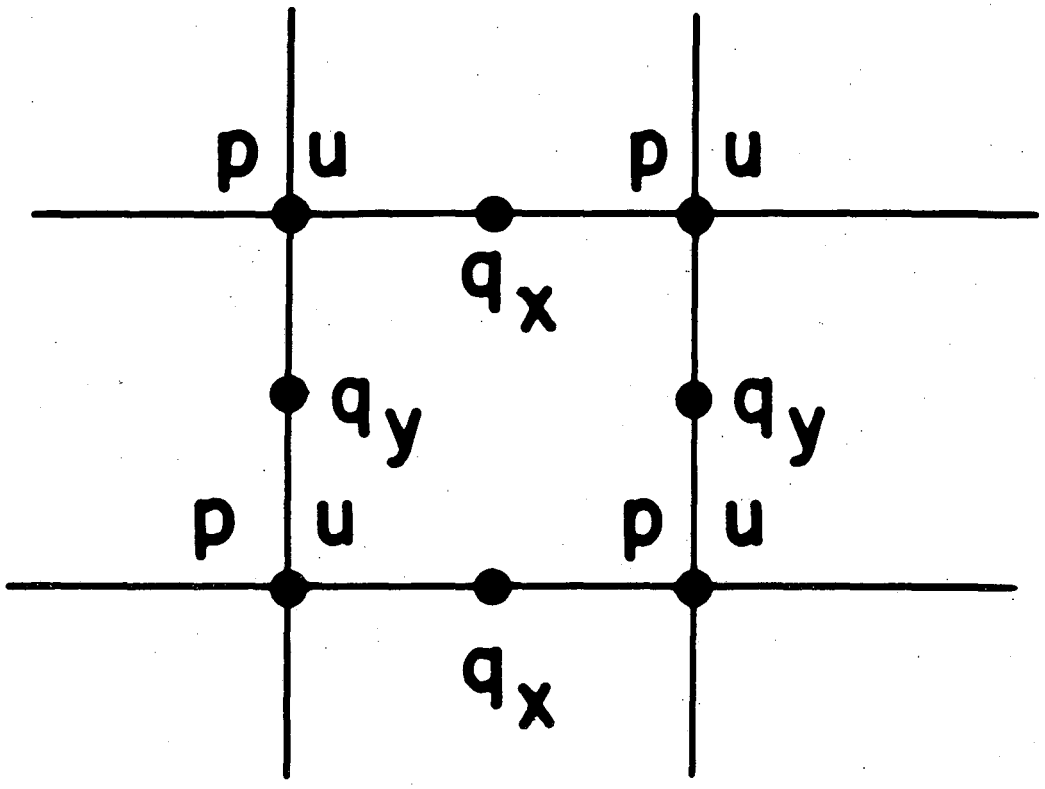

XBL 818-1232

Fig. 3.

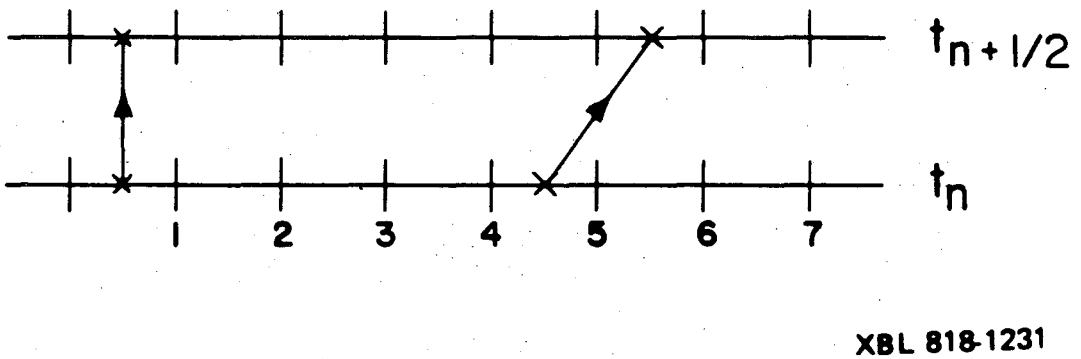

Fig. 4.

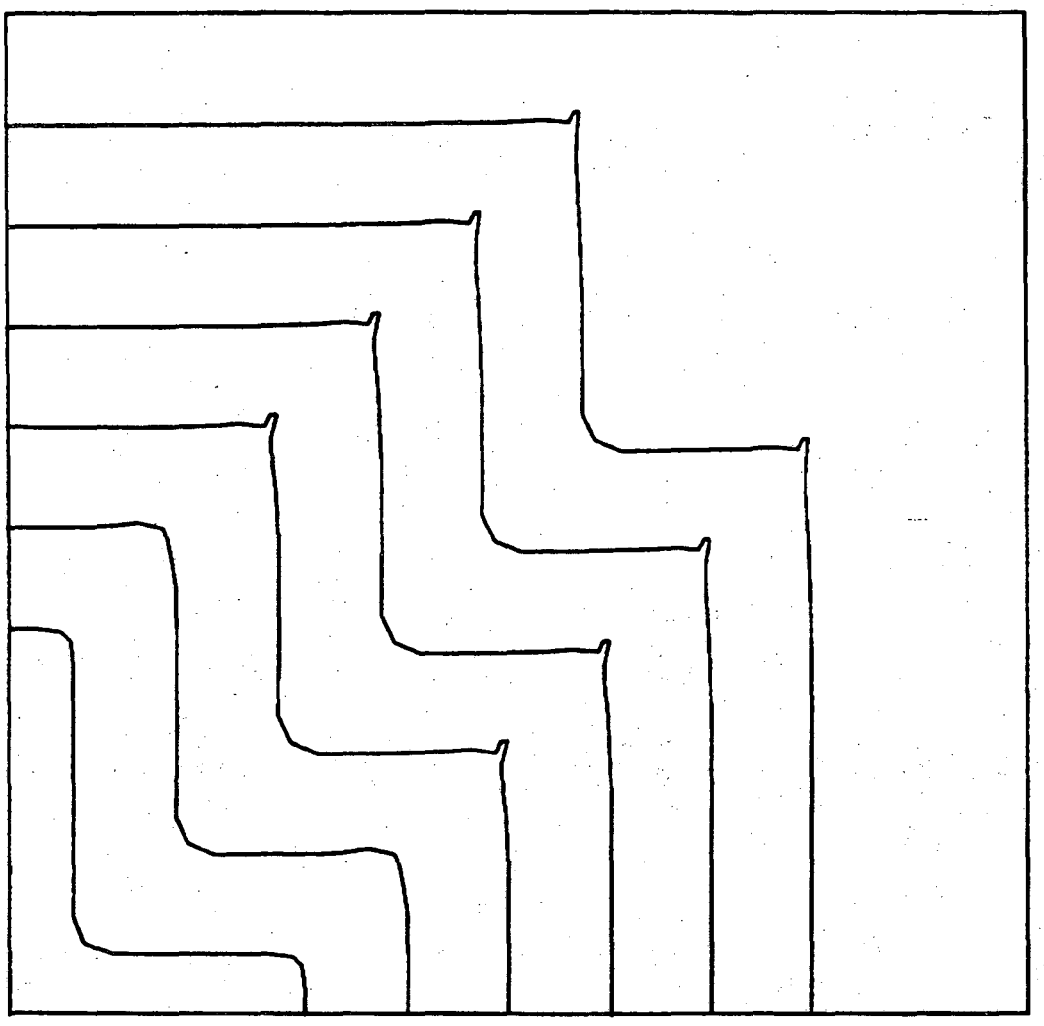

Fig. 5.

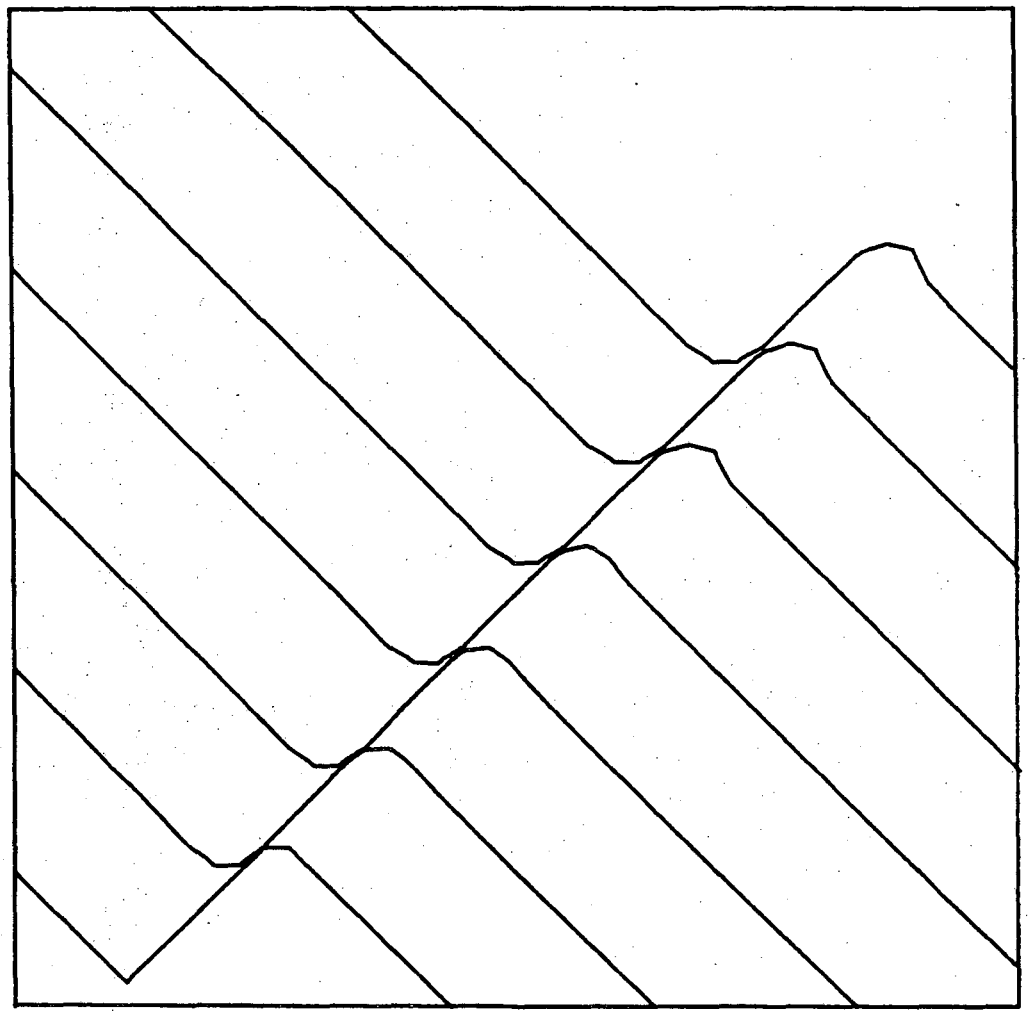

Fig. 6.

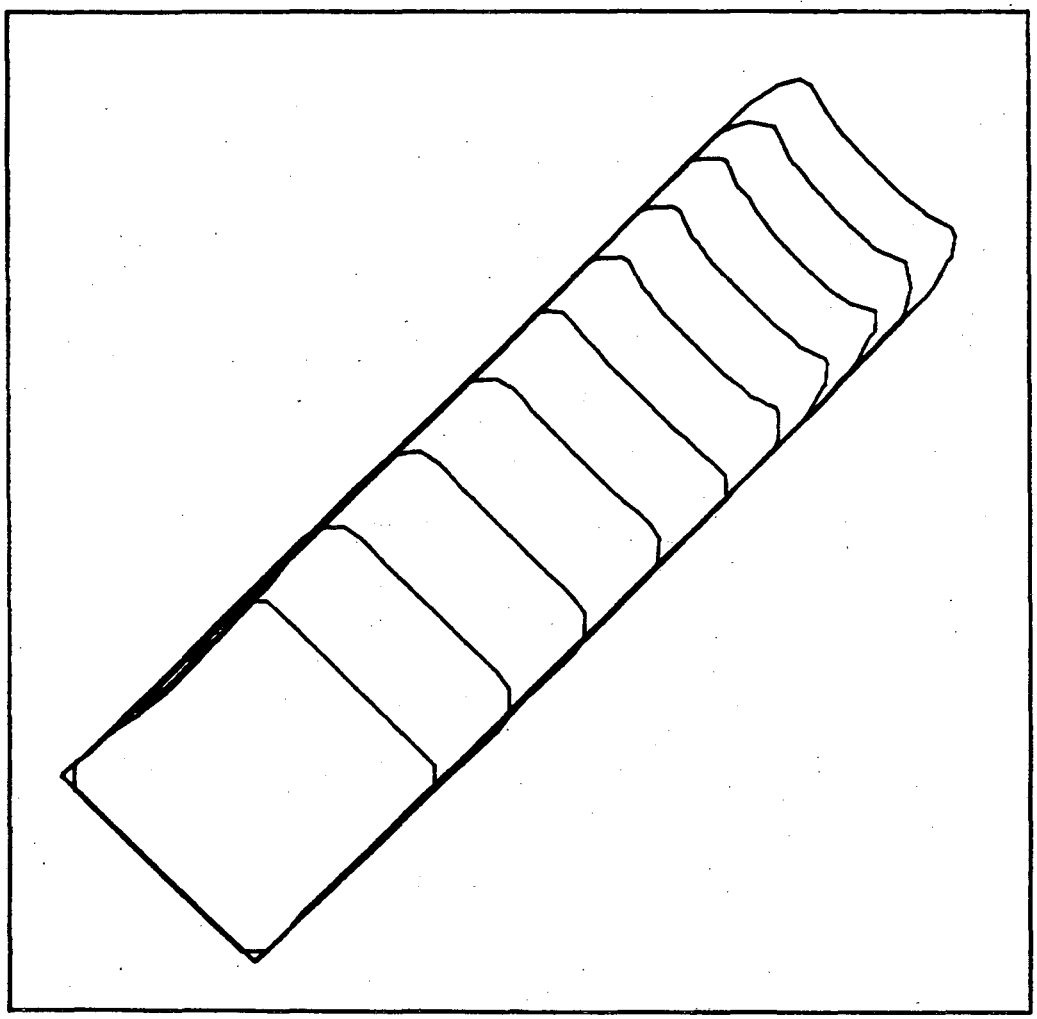

Fig. 7.

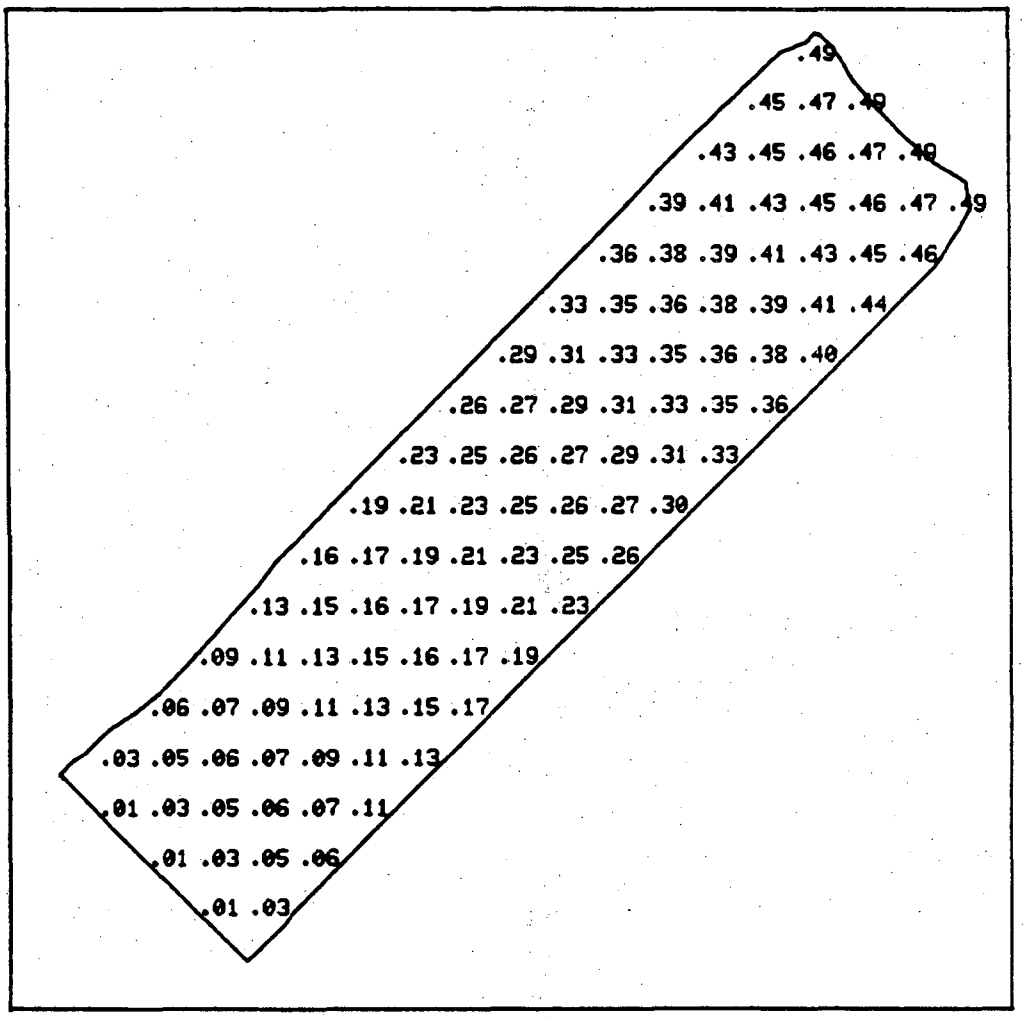
.49
.45 .47 .49
.43 .45 .46 .47 .49
.39 .41 .43 .45 .46 .47 .49
.36 .38 .39 .41 .43 .45 .46
.33 .35 .36 .38 .39 .41 .44
.29 .31 .33 .35 .36 .38 .40
.26 .27 .29 .31 .33 .35 .36
.23 .25 .26 .27 .29 .31 .33
.19 .21 .23 .25 .26 .27 .30
.16 .17 .19 .21 .23 .25 .26
.13 .15 .16 .17 .19 .21 .23
.09 .11 .13 .15 .16 .17 .19
.06 .07 .09 .11 .13 .15 .17
.03 .05 .06 .07 .09 .11 .13
.01 .03 .05 .06 .07 .11
.01 .03 .05 .06
.01 .03

Fig. 8.

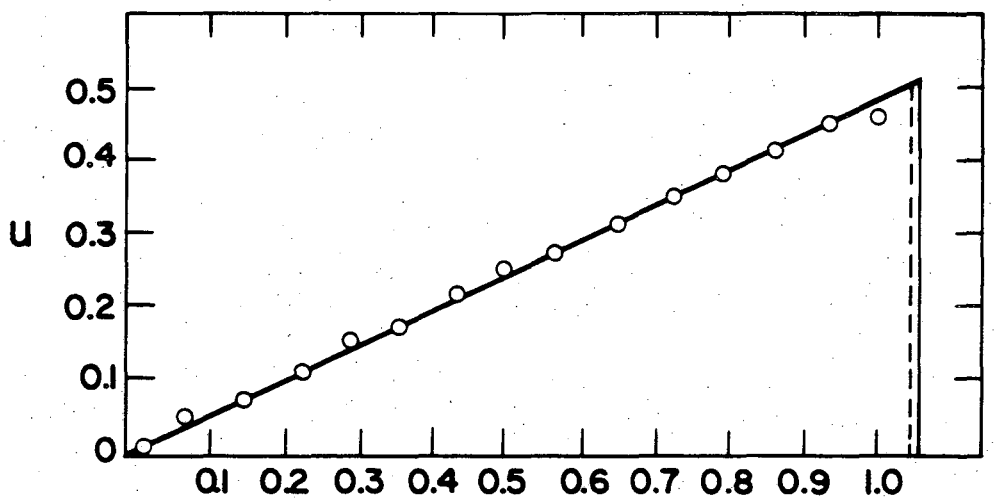

XBL 818-1230

Fig. 9.

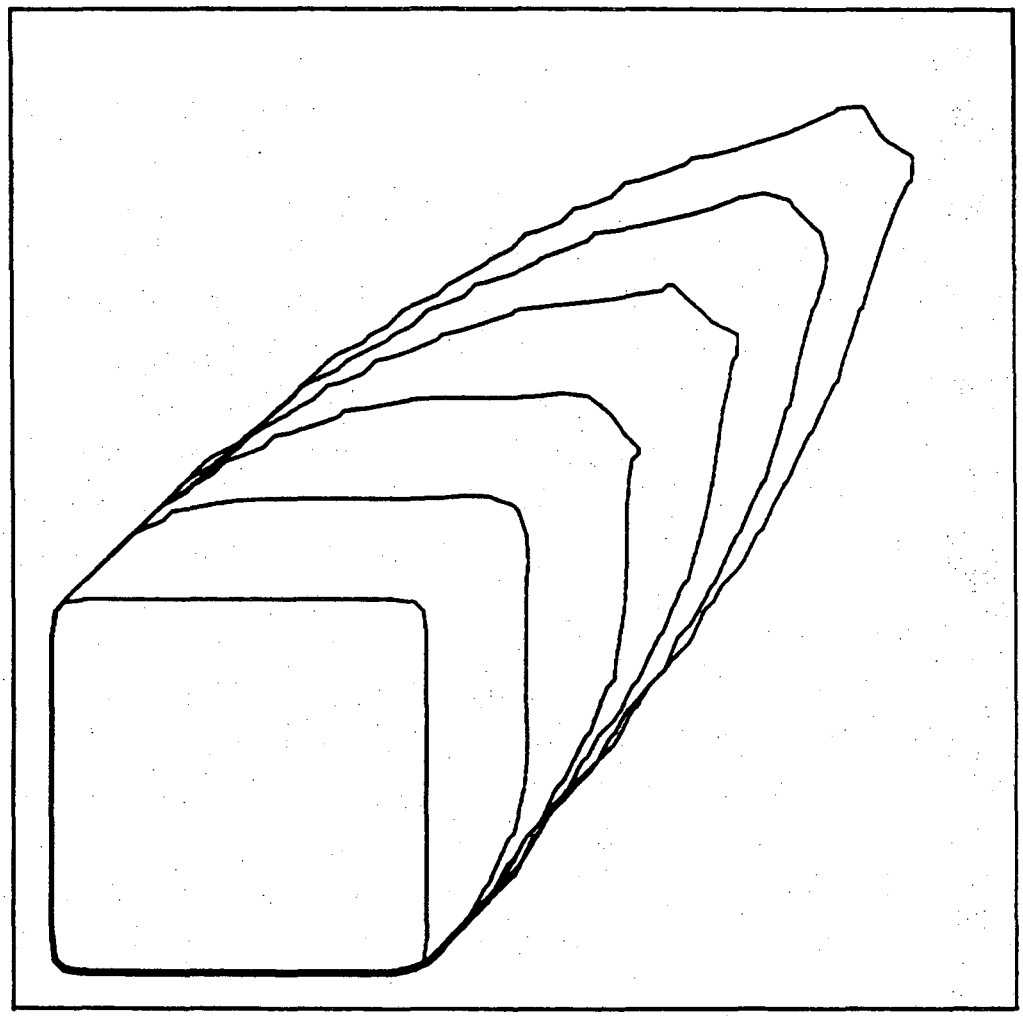

Fig. 10.

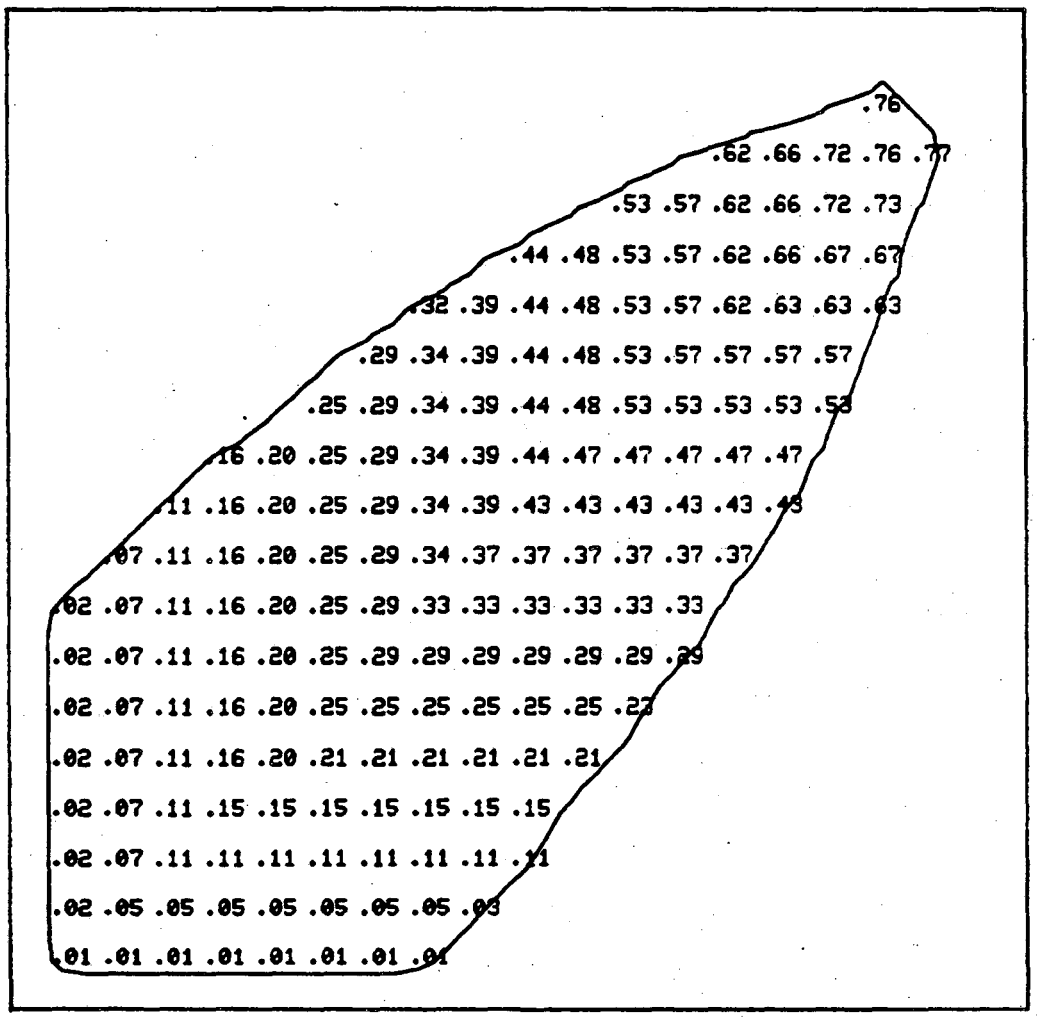
.76
.62 .66 .72 .76 .77
.53 .57 .62 .66 .72 .73
.44 .48 .53 .57 .62 .66 .67 .67
.32 .39 .44 .48 .53 .57 .62 .63 .63 .63
.29 .34 .39 .44 .48 .53 .57 .57 .57 .57
.25 .29 .34 .39 .44 .48 .53 .53 .53 .53 .53
.16 .20 .25 .29 .34 .39 .44 .47 .47 .47 .47 .47
.11 .16 .20 .25 .29 .34 .39 .43 .43 .43 .43 .43 .43
.07 .11 .16 .20 .25 .29 .34 .37 .37 .37 .37 .37 .37
.02 .07 .11 .16 .20 .25 .29 .33 .33 .33 .33 .33 .33
.02 .07 .11 .16 .20 .25 .29 .29 .29 .29 .29 .29 .29
.02 .07 .11 .16 .20 .25 .25 .25 .25 .25 .25 .23
.02 .07 .11 .16 .20 .21 .21 .21 .21 .21 .21
.02 .07 .11 .15 .15 .15 .15 .15 .15 .15
.02 .07 .11 .11 .11 .11 .11 .11 .11 .11
.02 .05 .05 .05 .05 .05 .05 .05 .03
.01 .01 .01 .01 .01 .01 .01 .01

Fig. 11.

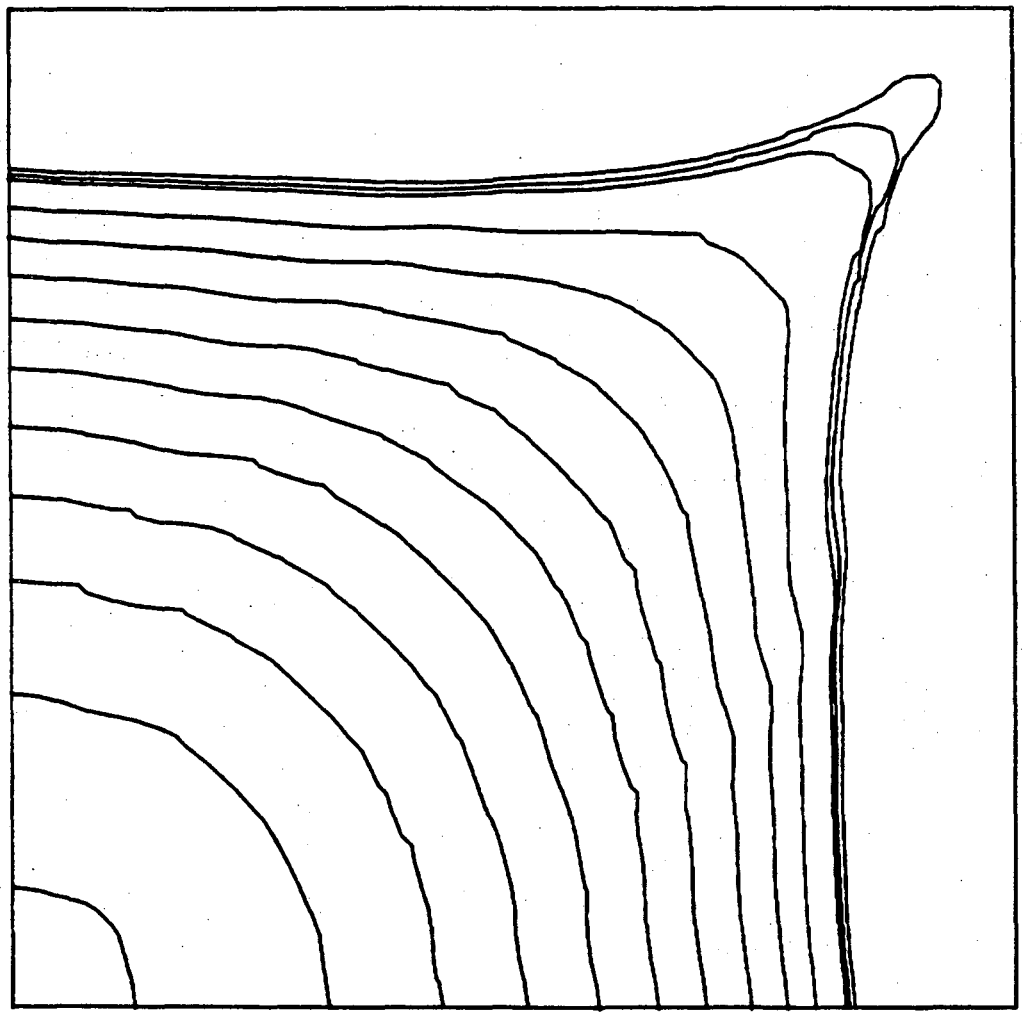

Fig. 12.

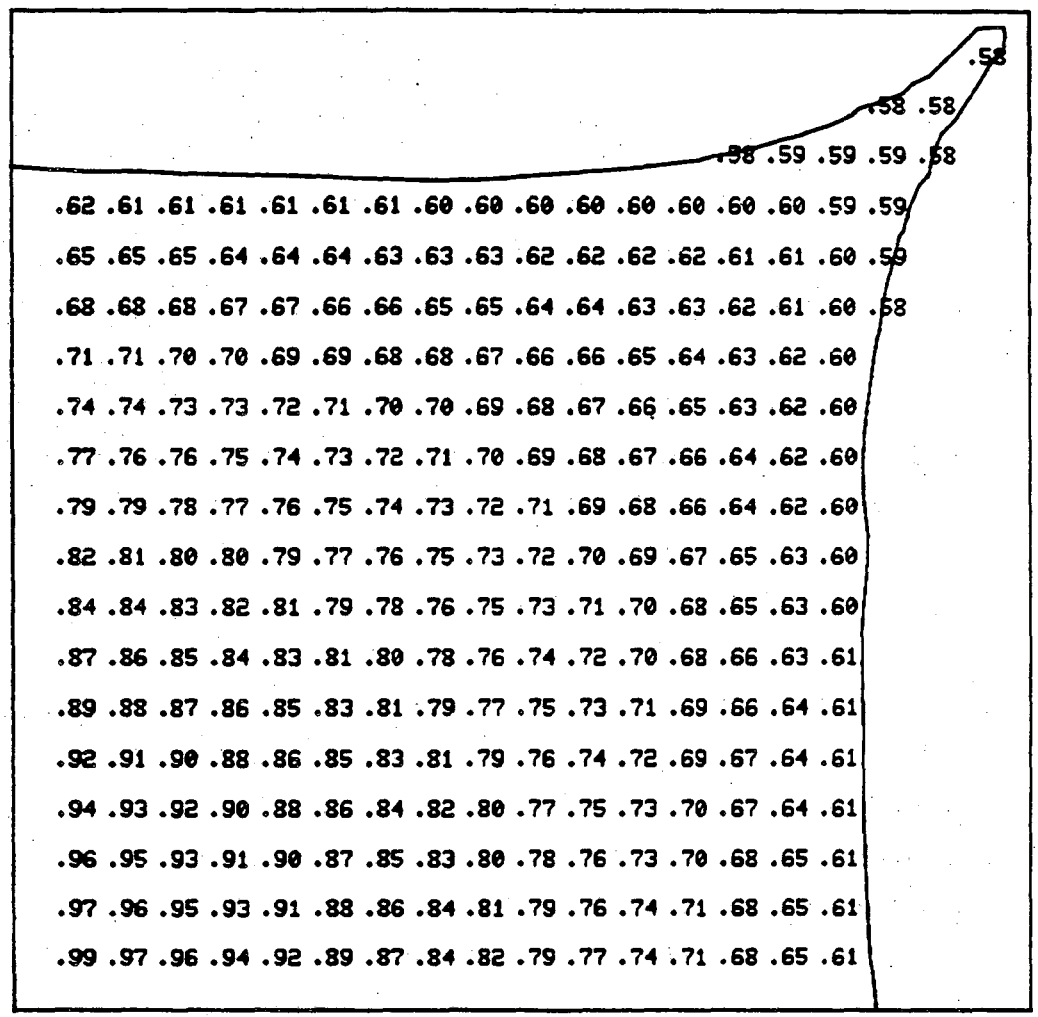
.58
.58 .58
.58 .59 .59 .59 .58
.62 .61 .61 .61 .61 .61 .61 .60 .60 .60 .60 .60 .60 .60 .60 .59 .59
.65 .65 .65 .64 .64 .64 .63 .63 .63 .62 .62 .62 .62 .61 .61 .60 .59
.68 .68 .68 .67 .67 .66 .66 .65 .65 .64 .64 .63 .63 .62 .61 .60 .58
.71 .71 .70 .70 .69 .69 .68 .68 .67 .66 .66 .65 .64 .63 .62 .60
.74 .74 .73 .73 .72 .71 .70 .70 .69 .68 .67 .66 .65 .63 .62 .60
.77 .76 .76 .75 .74 .73 .72 .71 .70 .69 .68 .67 .66 .64 .62 .60
.79 .79 .78 .77 .76 .75 .74 .73 .72 .71 .69 .68 .66 .64 .62 .60
.82 .81 .80 .80 .79 .77 .76 .75 .73 .72 .70 .69 .67 .65 .63 .60
.84 .84 .83 .82 .81 .79 .78 .76 .75 .73 .71 .70 .68 .65 .63 .60
.87 .86 .85 .84 .83 .81 .80 .78 .76 .74 .72 .70 .68 .66 .63 .61
.89 .88 .87 .86 .85 .83 .81 .79 .77 .75 .73 .71 .69 .66 .64 .61
.92 .91 .90 .88 .86 .85 .83 .81 .79 .76 .74 .72 .69 .67 .64 .61
.94 .93 .92 .90 .88 .86 .84 .82 .80 .77 .75 .73 .70 .67 .64 .61
.96 .95 .93 .91 .90 .87 .85 .83 .80 .78 .76 .73 .70 .68 .65 .61
.97 .96 .95 .93 .91 .88 .86 .84 .81 .79 .76 .74 .71 .68 .65 .61
.99 .97 .96 .94 .92 .89 .87 .84 .82 .79 .77 .74 .71 .68 .65 .61

Fig. 13.

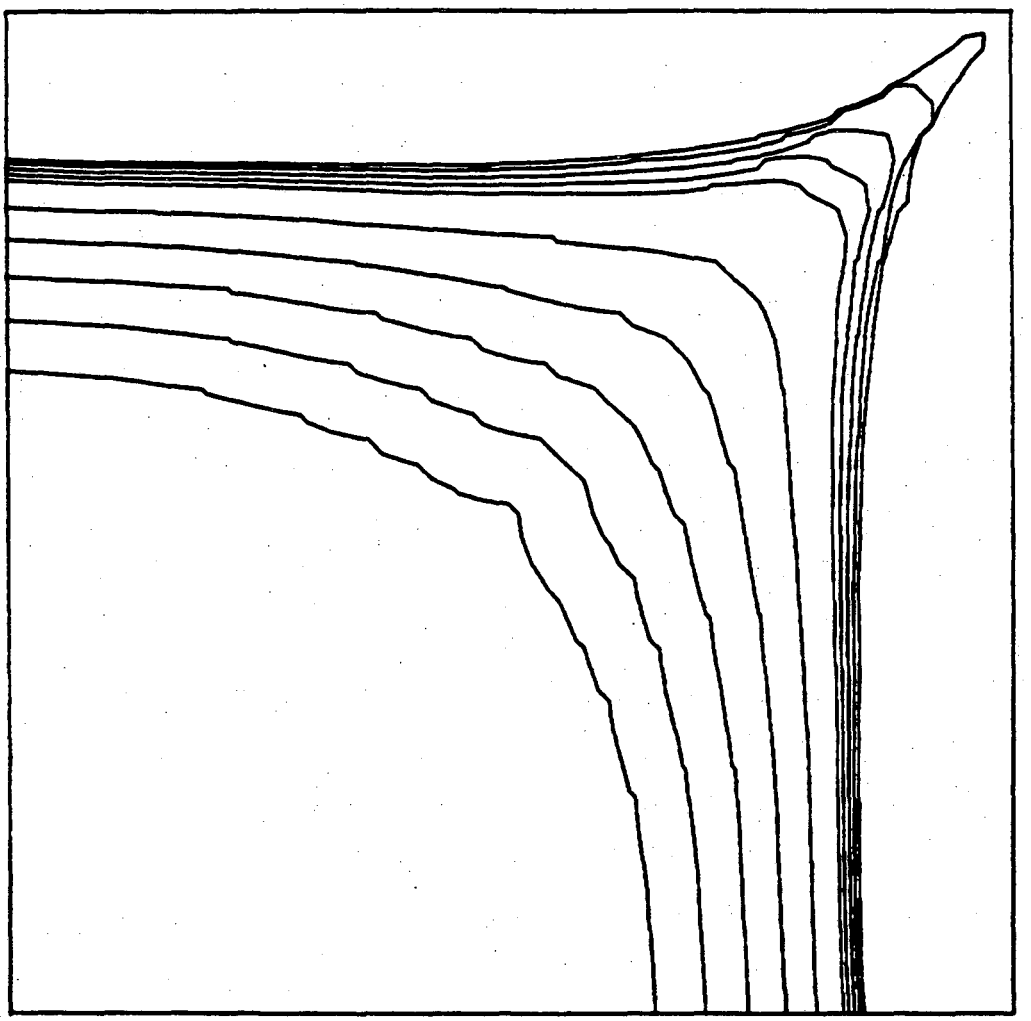

Fig. 14.

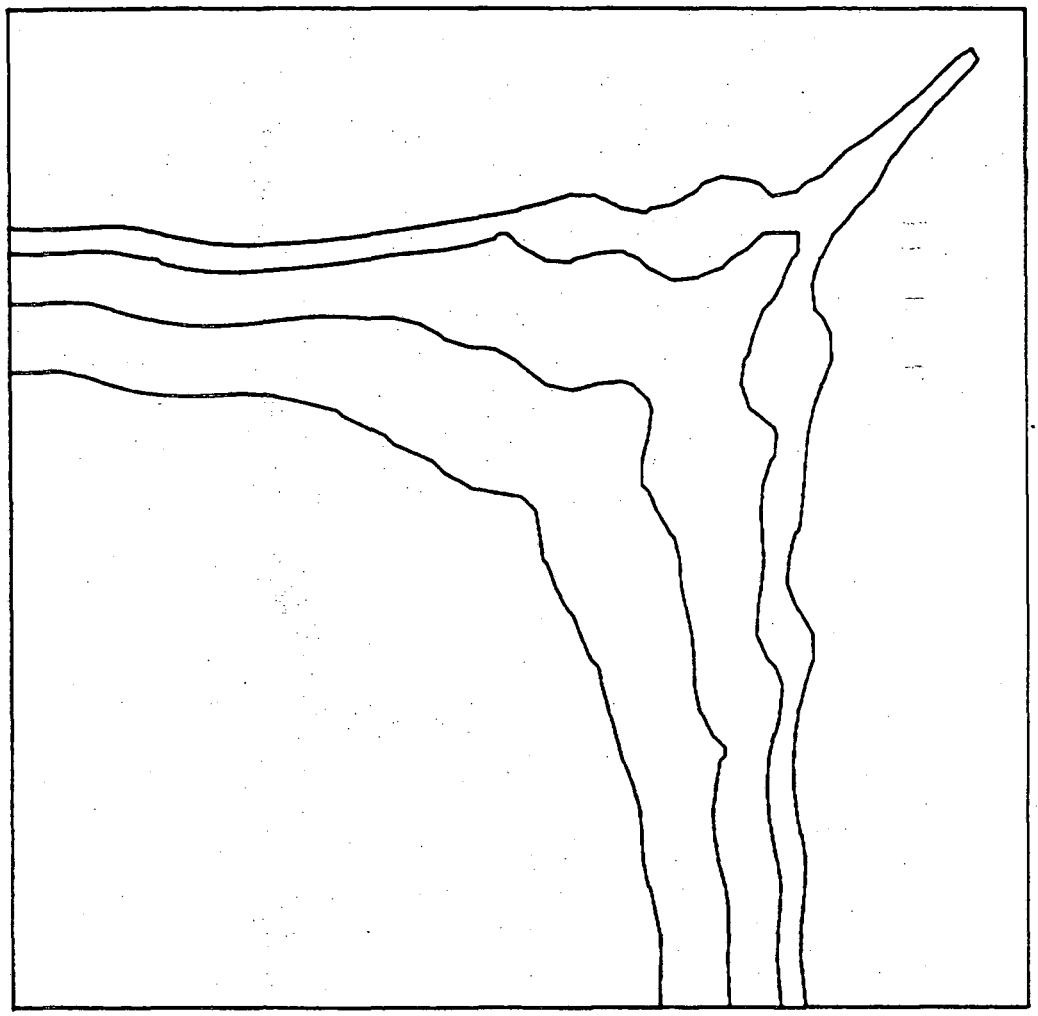

Fig. 15.

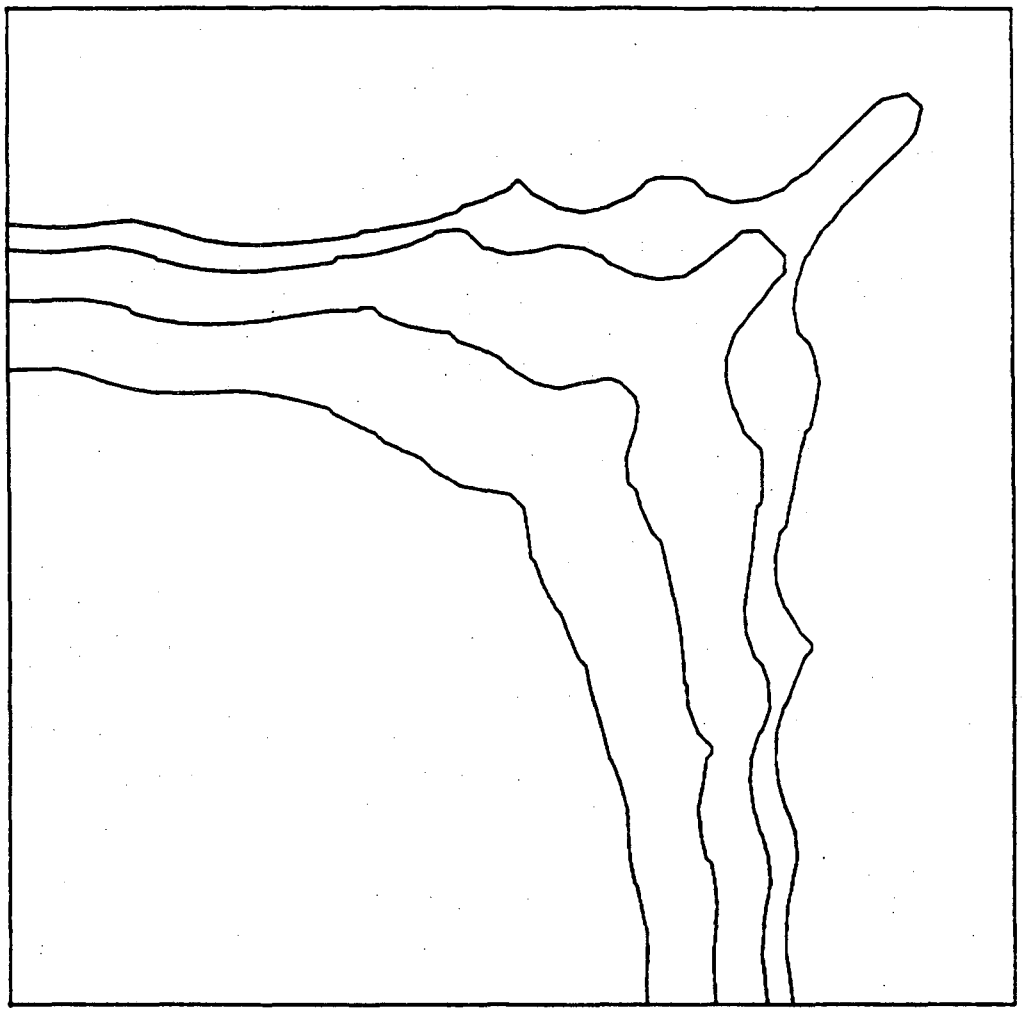

Fig. 16.

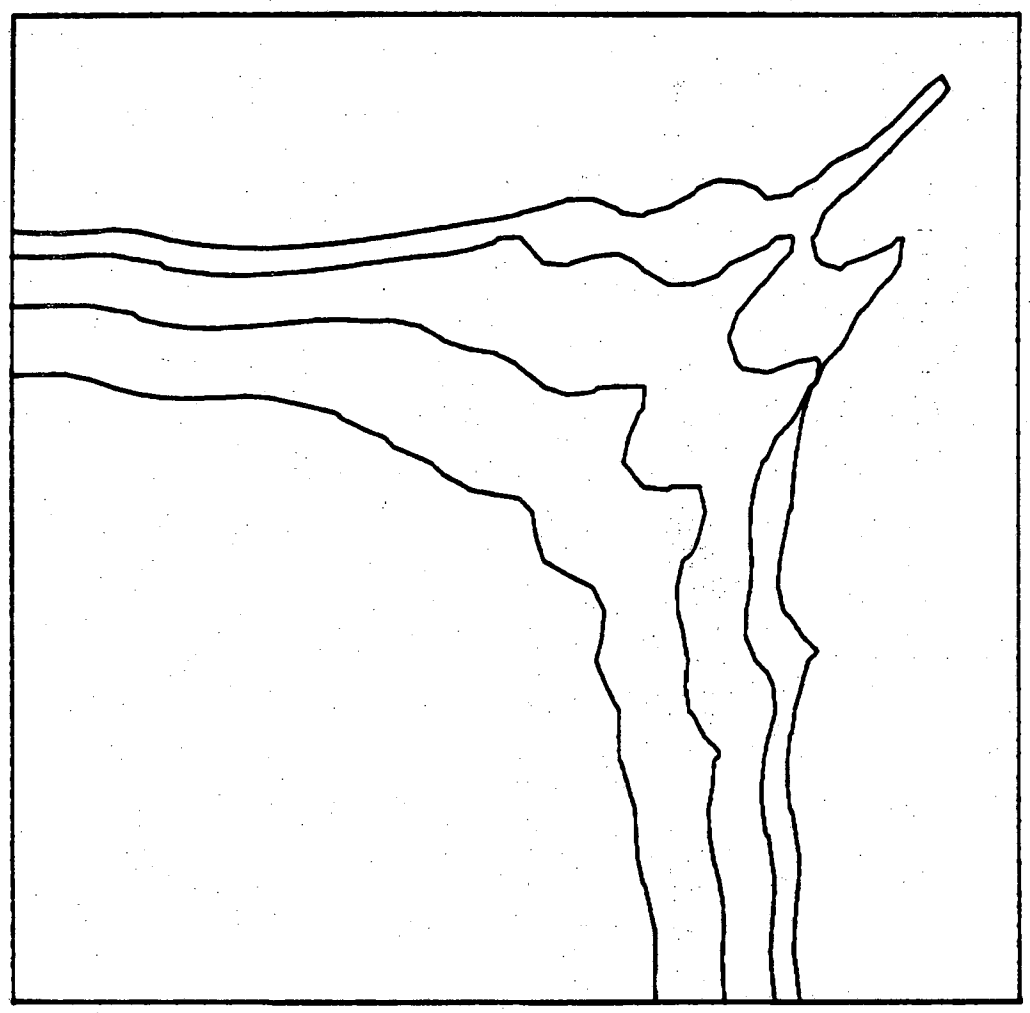

Fig. 17.

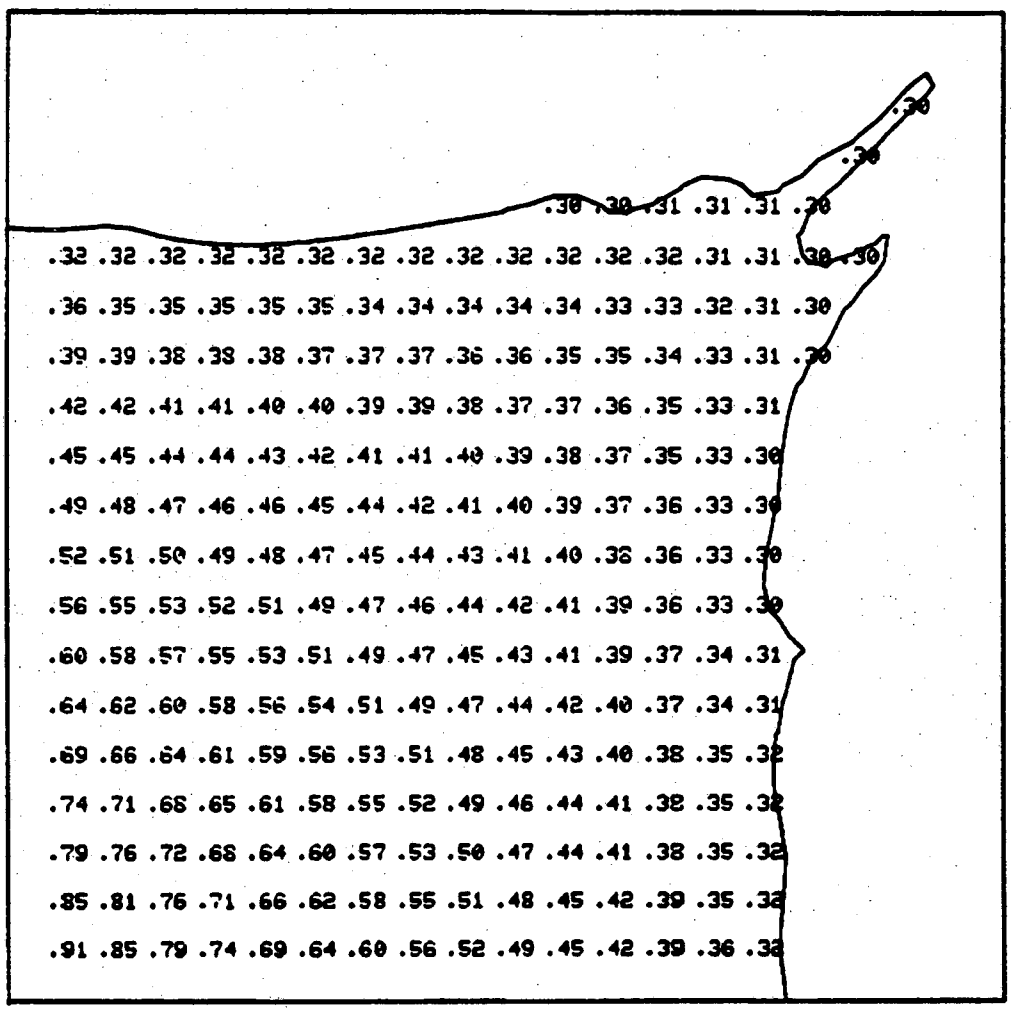
.30 .30
.30
.30 .30 .31 .31 .31 .30
.32 .32 .32 .32 .32 .32 .32 .32 .32 .32 .32 .32 .32 .31 .31 .30 .30
.36 .35 .35 .35 .35 .35 .34 .34 .34 .34 .34 .33 .33 .32 .31 .30
.39 .39 .38 .38 .38 .37 .37 .37 .36 .36 .35 .35 .34 .33 .31 .30
.42 .42 .41 .41 .40 .40 .39 .39 .38 .37 .37 .36 .35 .33 .31
.45 .45 .44 .44 .43 .42 .41 .41 .40 .39 .38 .37 .35 .33 .30
.49 .48 .47 .46 .46 .45 .44 .42 .41 .40 .39 .37 .36 .33 .30
.52 .51 .50 .49 .48 .47 .45 .44 .43 .41 .40 .38 .36 .33 .30
.56 .55 .53 .52 .51 .49 .47 .46 .44 .42 .41 .39 .36 .33 .30
.60 .58 .57 .55 .53 .51 .49 .47 .45 .43 .41 .39 .37 .34 .31
.64 .62 .60 .58 .56 .54 .51 .49 .47 .44 .42 .40 .37 .34 .31
.69 .66 .64 .61 .59 .56 .53 .51 .48 .45 .43 .40 .38 .35 .32
.74 .71 .68 .65 .61 .58 .55 .52 .49 .46 .44 .41 .38 .35 .32
.79 .76 .72 .68 .64 .60 .57 .53 .50 .47 .44 .41 .38 .35 .32
.85 .81 .76 .71 .66 .62 .58 .55 .51 .48 .45 .42 .39 .35 .32
.91 .85 .79 .74 .69 .64 .60 .56 .52 .49 .45 .42 .39 .36 .32

Fig. 18.

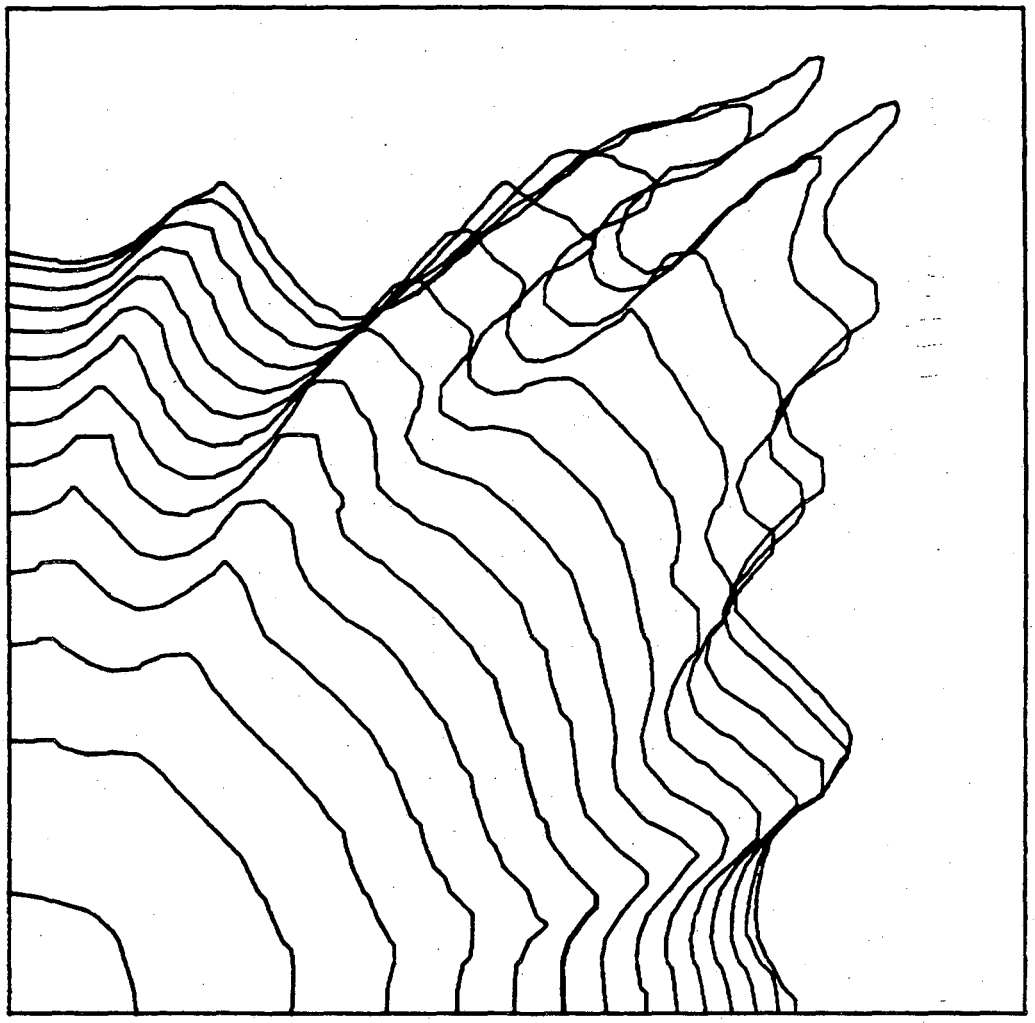

Fig. 19.

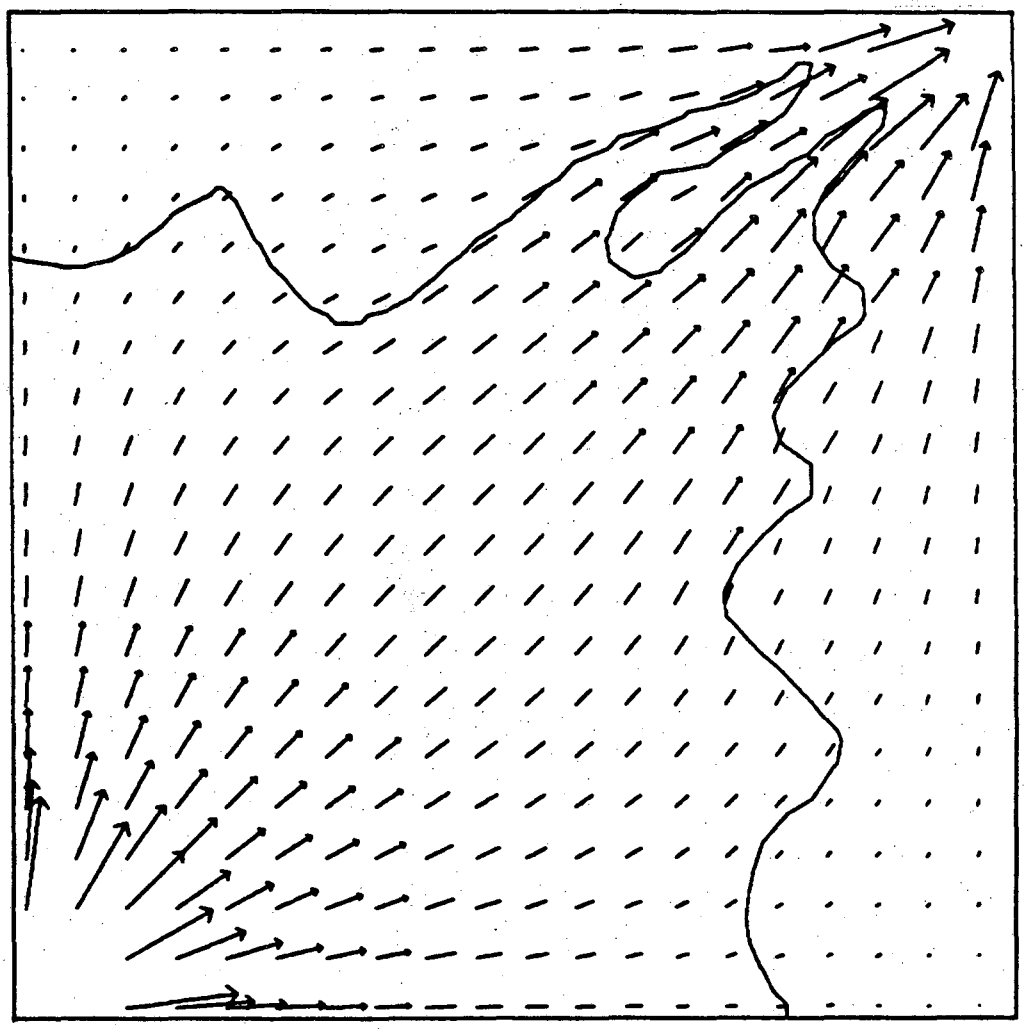

Fig. 20.

This report was done with support from the Department of Energy. Any conclusions or opinions expressed in this report represent solely those of the author(s) and not necessarily those of The Regents of the University of California, the Lawrence Berkeley Laboratory or the Department of Energy.

Reference to a company or product name does not imply approval or recommendation of the product by the University of California or the U.S. Department of Energy to the exclusion of others that may be suitable.

TECHNICAL INFORMATION DEPARTMENT
LAWRENCE BERKELEY LABORATORY
UNIVERSITY OF CALIFORNIA
BERKELEY, CALIFORNIA 94720